Altered conductance and permeability of Cx40 mutations associated with atrial fibrillation

Ana Santa Cruz, Gülistan Meşe, Laima Valiuniene, Peter R. Brink, Thomas W. White, and Virginijus Valiunas

Department of Physiology and Biophysics, Stony Brook University, Stony Brook, NY 11792

Gap junctions ensure the rapid propagation of the action potential throughout the myocardium. Three mutant forms of connexin40 (Cx40; A96S, M163V, and G38D), the primary component of the atrial gap junction channel, are associated with atrial fibrillation and retain the ability to form functional channels. We determined the biophysical properties of these mutant gap junctions in transiently transfected HeLa and N2A cells. All three mutants showed macroscopic junctional conductances over the range of 0.5 to 40 nS, and voltage dependences comparable to those of wild-type (WT) Cx40. However, the unitary conductance of G38D channels was ∼1.6-fold higher than that of WT Cx40 channels (∼220 vs. ∼135 pS), whereas the unitary conductances of the A96S and M163V mutants were similar to that of WT Cx40. Furthermore, the M163V and G38D channels exhibited approximately two- and approximately fivefold higher permeability to the anionic dye Lucifer yellow (LY) relative to K^+ (LY/K^+) compared with that of WT Cx40, whereas A96S LY transfer was similar to that of WT (G38D > M163V > A96S ≈ Cx40WT). In contrast, G38D channels were almost impermeable to cationic ethidium bromide (EtBr), suggesting that G38D alters channel selectivity. Conversely, A96S and M163V channels showed enhanced EtBr permeability relative to WT Cx40, with the following permeability order: M163V > A96S > Cx40WT > G38D. Altered conductive and permeability properties of mutant channels suggest an essential role for Cx40-mediated biochemical and electrical coupling in cardiac tissues. The altered properties of the three single-base substitution mutants may play a role in mechanisms of reentry arrhythmias.

The Journal of General Physiology

INTRODUCTION

Atrial fibrillation is often associated with cardiovascular diseases such as hypertension, ischemia-induced infarcts, and diabetes, all of which can lead to structural alterations of the atrial myocardium. However, a significant subset of patients suffering from atrial fibrillation show no such signs, where atrial fibrillation occurs spontaneously with little or no preconditioning or structural correlate (Saffitz, 2006). Genetic mutation is highly suspect in these patients, and membrane proteins associated with the conduction of the action potential are the primary suspects (Roberts, 2006).

The conduction of the cardiac action potential is generated by Cav 1.2 L-type calcium channels, Nav 1.5 sodium channels, and a battery of potassium channels aided by gap junction channels to ensure rapid propagation from cell to cell through the various regions of the myocardium. The type and number of gap junction channels and their distribution within myocytes can affect propagation (Kostin et al., 2002; Jansen et al., 2010). Gap junction channels within the atrial myocardium are composed predominately of connexin40 (Cx40) (Gros et al., 1994; Davis et al., 1995; Jansen et al., 2010) with lesser amounts of Cx43 and Cx45 (Kanter et al., 1993; Vozzi et al., 1999; Jansen et al., 2010).

Gollob et al. (2006) hypothesized that spontaneously arising atrial fibrillation might be the result of mutations within Cx40 and indeed found four heterozygous single-base substitutions in four individuals out of a sampling of 15 persons with spontaneous atrial fibrillation. In vitro studies demonstrated that one mutant, Pro-88-Ser, did not traffic to the membrane, and hence no functional channels were formed. The other three mutants, Ala96-Ser (A96S), Met163-Val (M163V), and Gly38-Asp (G38D), were shown to form functional gap junction plaques in cell pairs with macroscopic conductance ranging from an average of 1.8 nS for A96S to 17.8 nS for M163V (Gollob et al., 2006). The former of these two was significantly less than the WT control, whereas the latter was equivalent. Furthermore, coexpression of A96S with WT Cx40 demonstrated a dominant-negative effect. These data suggested that a closer inspection of the biophysical properties might provide answers with regard to the potential of these mutant forms to participate in arrhythmogenic processes

Correspondence to Virginijus Valiunas: virginijus.valiunas@stonybrook.edu

G. Meşe's present address is Dept. of Molecular Biology and Genetics, Izmir Institute of Technology, 35430 Izmir, Turkey.

Abbreviations used in this paper: Cx40, connexin40; EtBr, ethidium bromide; LY, Lucifer yellow.

The Rockefeller University Press $30.00
J. Gen. Physiol. Vol. 146 No. 5 387–398
www.jgp.org/cgi/doi/10.1085/jgp.201511475

associated with atrial fibrillation. A recent study by Christophersen et al. (2013) has also demonstrated lone atrial fibrillation associated with the A96S mutation of human Cx40.

We transfected cDNA for A96S, M163V, and G38D into connexin-deficient HeLa and N2A cells. All three mutants trafficked to the membrane and formed plaques. Dual whole-cell patch clamp was used to compare both the unitary conductance of the mutant forms and their permeability characteristics to larger molecules, with WT Cx40 (Valiunas et al., 2002; Kanaporis et al., 2008, 2011). None of the mutants affected voltage-dependent gating. Two of the mutants had unitary conductances that were similar to that of WT, whereas G38D was significantly higher (1.6 times the WT). All three mutants had significantly different permeability characteristics relative to WT Cx40.

MATERIALS AND METHODS

Cells and culture conditions

Experiments were performed using HeLa and N2A cells that were transfected with human Cx40 WT or the mutants A96S, G38D, and M163V cDNA. hCx40 WT or mutant cDNAs were subcloned into the eukaryotic expression vector pIRES2-EGFP (Takara Bio Inc.). Cells were transiently transfected using Lipofectamine 2000 (Invitrogen) reagent according to the manufacturer's protocol. The cells were grown in DMEM (Gibco), supplemented with 10% FCS (Hyclone), 100 µg/ml streptomycin (Gibco), and 100 U/ml penicillin (Gibco), and were then passaged weekly, diluted at 1:10, and kept at 37°C in a CO_2 incubator (5% CO_2/95% ambient air). Immunofluorescent staining, electrophysiological measurements, and dye flux studies were performed on cell pairs cultured for 1–3 d.

Immunofluorescent staining

HeLa cells were grown on glass coverslips and transiently transfected with pIRES2-EGFP Cx40 WT and mutant constructs. 24 h after transfection, cells were fixed with 1% paraformaldehyde in PBS for 15 min, permeabilized with PBS-0.1%Triton X-100 for 10 min, and then blocked with 3% BSA in PBS-0.1% Triton X-100 for 30 min at room temperature. A 1:100 dilution of a polyclonal rabbit anti-Cx40 antibody (Santa Cruz Biotechnology, Inc.) was applied for 1 h. Then, cells were treated with a 1:2,000 dilution of secondary Cy3-conjugated goat anti–rabbit antibody (AffiniPure; Jackson ImmunoResearch Laboratories, Inc.) for 30 min in the dark. The coverslips were mounted on slides using Vectashield with DAPI (Vector Laboratories) and visualized with 40 or 60× objectives on a microscope (BX51; Olympus) and photographed with a digital camera (MagnaFire; Olympus).

Electrophysiological measurements

For simultaneous electrical and fluorescence recording, glass coverslips with adherent cells were transferred to an experimental chamber mounted on the stage of an inverted microscope (IX71; Olympus) equipped with a fluorescence imaging system. A dual voltage-clamp method and whole-cell recording were used to control the membrane potential of both cells and to measure the currents (Valiunas et al., 2001).

The chamber was perfused at room temperature (~22°C) with a bath solution containing (mM): 137.7 NaCl, 5.4 KCl, 2 $CaCl_2$, 1 $MgCl_2$, 5 HEPES, pH 7.4, 10 glucose, 2 CsCl, and 2 $BaCl_2$. The patch pipettes were filled with solution filtered through 0.22-µm pores containing (mM): 120 K^+ aspartate$^-$, 10 NaCl, 3 MgATP, 5 HEPES, pH 7.2, and 10 EGTA (pCa of ~8). Patch pipettes were pulled from glass capillaries (GC150F; Harvard Apparatus) with a horizontal puller (DMZ-Universal; Zeitz Instruments GmbH). When filled, the resistance of the pipettes measured 1–4 MΩ.

Dye flux studies

Dye transfer through gap junction channels was investigated using cell pairs. Lucifer yellow (LY; Molecular Probes) and ethidium bromide (EtBr; Molecular Probes) were dissolved in the pipette solution at a concentration of 1 mg/ml. The transfer of dyes through gap junction channels was investigated by introducing fluorescent probes via a patch pipette to the one cell of a pair and then monitoring the change in fluorescence in both cells over time, simultaneously measuring junctional conductance, as mentioned previously (Valiunas et al., 2002; Kanaporis et al., 2011). To prevent dye washout, the recipient cell was held in perforated patch-clamp mode (Valiunas et al., 2002). For perforated-patch experiments, 30–50 µM β-escin was added to the pipette-filling solution (Fan and Palade, 1998).

The cell-to-cell spread of LY and EtBr dyes was imaged using a 14-bit digital CCD camera (HRm Axiocam; Carl Zeiss). The fluorescence intensities in both recipient and donor cells were measured over the time and corrected by subtracting the background fluorescence intensity. The relative fluorescence intensity was calculated as a ratio of the fluorescence intensity in the recipient cell over the fluorescence intensity in the injected cell, using measurements taken 12 min after the application of the dye. Dye flux (molecules/channel/s), unitary channel permeability (Pγ), and the ratio between dye flux and the permeability of the channel to ubiquitous monovalent ion K^+ were calculated as described previously (Valiunas et al., 2002; Hernandez et al., 2007; Kanaporis et al., 2008, 2011).

Signal recording and analysis

Voltage and current signals were recorded using patch-clamp amplifiers (Axopatch 200; Molecular Devices). The current signals were digitized with a 16-bit A/D converter (Digidata 1440A; Molecular Devices) and stored within a personal computer. Data acquisition and analysis were performed with pClamp9 software (Molecular Devices). Curve fitting and statistical analyses were performed using SigmaPlot and SigmaStat, respectively (Systat Software Inc.). The results are presented as means ± 1 SEM.

RESULTS

Localization of mutant Cx40 proteins within cells

Connexin-deficient HeLa cells were transiently transfected with pIRES2-EGFP constructs with hCx40 WT or the mutants A96S, G38D, and M163V. Fig. 1 A depicts the relative position of each mutation site, with G38D in the first transmembrane domain M1, and then A96S in M2 and M163V in M3. Immunofluorescent staining with anti-Cx40 antibodies verified protein expression and localization for WT and mutant forms of hCx40, as shown in Fig. 1 B. All three mutant proteins exhibited an expression in a manner comparable to WT Cx40, and in every case, gap junction plaques were observed at cell–cell interfaces (Fig. 1 B).

Functional properties of Cx40 mutant gap junctions

Electrical coupling and voltage gating. To test whether mutant connexins form functional gap junction channels, transiently transfected HeLa and N2A cells were

investigated using dual whole-cell patch clamp. All three mutants exhibited a range of macroscopic junctional conductance (g_j) ranging from 0.5 to 40 nS, as summarized in Table 1. All transfectants, except hCx40WT, exhibited slightly lower macroscopical conductances in N2A cells versus HeLa cells (Table 1), but the differences were not statistically significant. Also, none of the mutations showed a significantly lower junctional conductance relative to hCx40WT. This, though, was not the case with the study performed by Gollob et al. (2006), where A96S mutants showed a significantly reduced average junctional conductance relative to Cx40 WT. However, all mutant and hCx40WT transient transfectants exhibited significantly lower junctional conductances when compared with a stably transfected rat Cx40WT HeLa cell line (see Table 1).

The relationship between transjunctional voltage (V_j) and g_j was studied systematically in HeLa cell pairs transfected with Cx40 mutants: A96S, G38D, and M163V. Both cells of a pair were clamped to the same holding potential (V_h). Starting from a V_h of 0 mV, bipolar pulses of 2-s duration were administered to establish V_j gradients of identical amplitude with either polarity. V_j was then changed from ±10 to ±110 mV using increments of 20 mV (Fig. 2). Fig. 2 (A–C, left panels) shows recordings from pairs of HeLa Cx40A96S, Cx40G38D, and Cx40M163V transfectants. The associated gap junction currents (I_j) increased proportionally with V_j and exhibited a voltage- and time-dependent deactivation for positive and negative V_j. The current amplitudes were determined at the beginning ($I_{j,inst}$) and the end of each pulse ($I_{j,ss}$), and the values of normalized junctional conductance ($g_{j,norm}$) were plotted versus V_j. The right panels of Fig. 2 (A–C) summarize the data gathered from HeLa preparations transfected with Cx40 mutants. The normalized steady-state conductance from multiple experiments can be fit to a Boltzmann equation (continuous curve in Fig. 2, A–C) with the following parameters: half deactivation voltage ($V_{j,o}$ = 49, 48, and 52 mV), gating charge (z = 2.1, 2.1, and 3.1), and a voltage-insensitive component of g_j, ($g_{j,min}$ = 0.20, 0.20, and 0.22) for A96S, G38D,

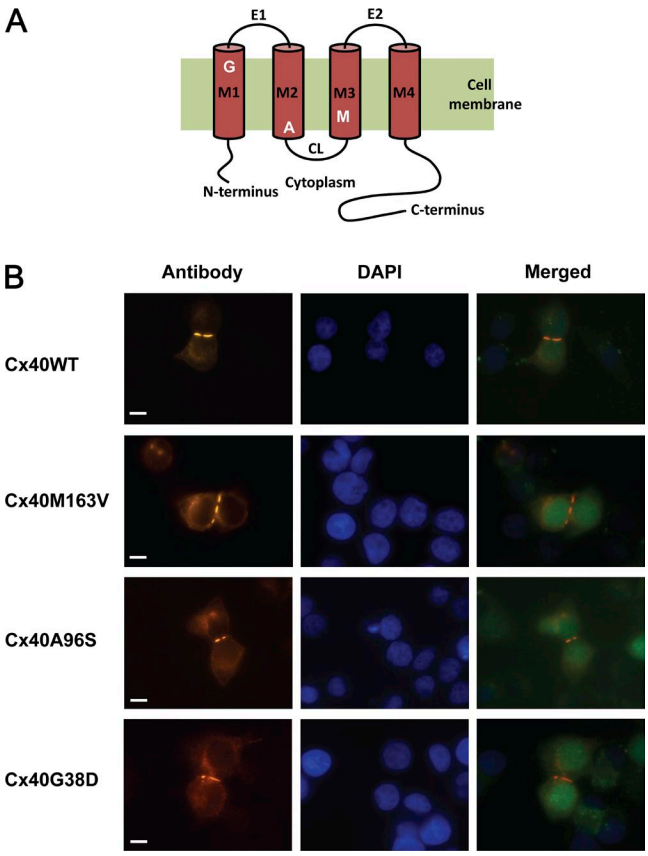

Figure 1. Localization of WT and mutant Cx40 proteins. (A) Schematic representation of Cx40 with three mutation sites. (B) HeLa cells stained with antibodies to Cx40 show typical punctate staining at regions of cell contact for WT and mutated connexins (M163V, A96S, and G38D). DAPI staining indicates cell locations, and EGFP fluorescence in merged images identifies transfected cells.

TABLE 1

Summary of conductance and permeability data collected from mutant and WT Cx40

	hCx40WT	rCx40WT	Cx40A96S	Cx40G38D	Cx40M163V
Junctional conductance (nS)					
HeLa	8.5 ± 0.6 (n = 32)	24.1 ± 3.5 (n = 22)	8.9 ± 1.5 (n = 34)	8.6 ± 0.9 (n = 51)	9.1 ± 1.0 (n = 38)
N2A	8.9 ± 1.8 (n = 18)	n.a.	7.3 ± 2.7 (n = 10)	8.3 ± 2.7 (n = 10)	7.2 ± 2.1 (n = 17)
Unitary conductance (pS)	135	125[a]	139	220	131
$V_{j,o}$ (mV)	48	48	49	52	48
z	3.9	4.1	2.1	2.1	3.1
$g_{j,min}$	0.24	0.24	0.20	0.20	0.22
LY flux (molec/channel/s)	989	650	1,137	7,758	2,242
Pγ (cm^3/s)	0.82×10^{-15}	0.54×10^{-15}	0.95×10^{-15}	6.52×10^{-15}	1.87×10^{-15}
LY/K^+	0.0030	0.0021	0.0034	0.0145	0.0070
EtBr flux (molec/channel/s)	5,059	5,454	16,156	1,121	19,218
Pγ (cm^3/s)	3.61×10^{-15}	3.35×10^{-15}	10.91×10^{-15}	0.73×10^{-15}	13.08×10^{-15}
EtBr/K^+	0.0131	0.0131	0.0376	0.0016	0.0474

n.a., not applicable.
[a]Valiunas et al. (2002).

and M163V, respectively. For comparison, the gray dashed lines in Fig. 2 (A–C, right panels) correspond to the Boltzmann fit of WT hCx40 data ($V_{j,o}$ = 48 mV, z = 3.9, and $g_{j,min}$ = 0.24). None of the mutants significantly altered voltage-dependent gating relative to the WT connexin as shown in Fig. 2. WT hCx40 exhibited voltage sensitivity that closely resembles results reported previously for rat and mouse Cx40 (Beblo et al., 1995; Bukauskas et al., 1995; Valiunas et al., 2001).

Single-channel properties. Single-channel properties were examined to look for differences in the unitary conductance between the mutant and WT connexins. To study single-channel currents, we selected weakly coupled N2A cell pairs that had one or two operational channels. Fig. 3 (A–C) illustrates these experiments, showing representative single-channel current recordings obtained from N2A cell pairs expressing Cx40 mutant connexins A96S, M163V, and G38D. The all-point current histograms revealed conductance levels of 139 pS for Cx40A96S (Fig. 3 A) and 140–144 pS for Cx40M163V (Fig. 3 B). In the case of Cx40G38D (Fig. 3 C), the channel gated between the main state and residual state (lowest dashed line). Analysis of the current amplitude histogram yielded a unitary channel conductance of 235 pS for the main state and 60 pS for the residual state. Fig. 3 D shows an exemplary record of a single-channel current for human WT Cx40 at a maintained voltage gradient of V_j = 50 mV. The current analysis revealed a unitary conductance of 138 pS. The unitary conductance data for all three mutants are summarized in Fig. 3 E. The unitary conductance of A96S (139 ± 2 pS) and M163V (131 ± 2 pS) was similar to the WT hCx40 (135 ± 2 pS), i.e., P = 0.111 and P = 0.059, respectively. However, G38D channels (220 ± 3 pS) were significantly more conductive than the WT Cx40 channels (P < 0.001).

Permeability of mutant channels to anionic and cationic probes. To examine the permeability of mutant connexins in this study, we used fluorescent probes with different

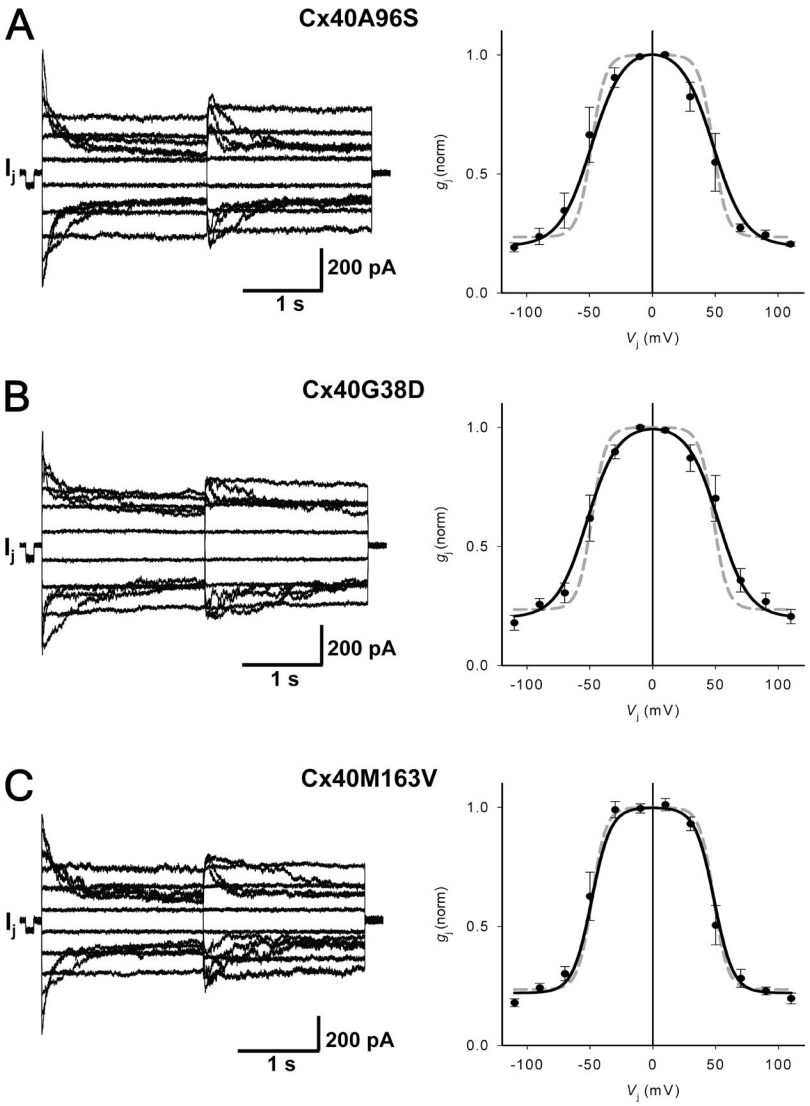

Figure 2. Macroscopic properties: voltage gating of Cx40 mutant gap junctions. (Left) Gap junction currents (I_j) elicited by a bipolar pulse protocol from HeLa cells transfected with Cx40 mutants: A96S (A), G38D (B), and M163V (C). (Right) Summary plots of normalized g_j versus V_j. The continuous black lines represent the best fit of the data to the Boltzmann equation: (A) A96S ($V_{j,o}$ = 49 mV, $g_{j,min}$ = 0.20, and z = 2.1; n = 5); (B) G38D ($V_{j,o}$ = 52 mV, $g_{j,min}$ = 0.20, and z = 2.1; n = 7); (C) M163V ($V_{j,o}$ = 48 mV, $g_{j,min}$ = 0.22, and z = 3.1; n = 10). The dashed gray line corresponds to the Boltzmann fit of Cx40 data ($V_{j,o}$ = 48 mV, $g_{j,min}$ = 0.24, and z = 3.9; n = 6). Error bars represent means ± SEM.

molecular weights. We compared the permeation of LY, an anionic probe, and EtBr, a cationic probe, through mutant channels expressed in HeLa cells, by using the experimental approach of simultaneously measuring cell-to-cell transfer of dye flux and junctional conductance (Fig. 4 A; Valiunas et al., 2002; Kanaporis et al., 2011). Fig. 4 B shows an example of LY diffusion in a HeLaCx40G38D cell pair. Fluorescence intensity was monitored in both the recipient and the donor cells over time after a patch electrode with a fluorescent probe was opened (Fig. 4 A). Fig. 4 C shows the fluorescence intensity values plotted versus time for source cell (●) and recipient cell (○). The junctional conductance (g_j) was monitored by recording the transjunctional current (I_j) generated in response to short (400-ms) 10-mV V_j, steps (Fig. 4 D, top). At the end of each experiment, 100% CO_2 was perfused into the bath to demonstrate junctional uncoupling, as shown in the bottom of Fig. 4 D, and to prove that dye diffused through gap junction channels and that cytoplasmic bridges (Bukauskas et al., 1992) were not present.

LY dye flux and g_j were examined in many mutant cell pairs. Fig. 4 E shows the summary data of these experiments, where the relative fluorescence intensity (a ratio of the recipient cell's fluorescence intensity to the source cell's fluorescence intensity) at the 12-min mark (shaded area in Fig. 4 C) is plotted against the measured junctional conductance for each experiment. LY permeability for WT rCx40 has been determined previously (Kanaporis et al., 2011) and recapitulated here. Linear fits of the data to first-order regression exhibited the following slopes: 0.0057 ± 0.0003 nS^{-1}, 0.0027 ± 0.0005 nS^{-1}, and 0.0117 ± 0.0012 nS^{-1} for M163V, A96S, and G38D mutants, respectively. WT hCx40 data produced a slope of 0.0024 ± 0.0005 nS^{-1}. Comparison of the slopes by analysis of covariance (GraphPad Prism) revealed that the differences between M163V, G38D, and WT hCx40 were statistically significant (P = 0.0035 and

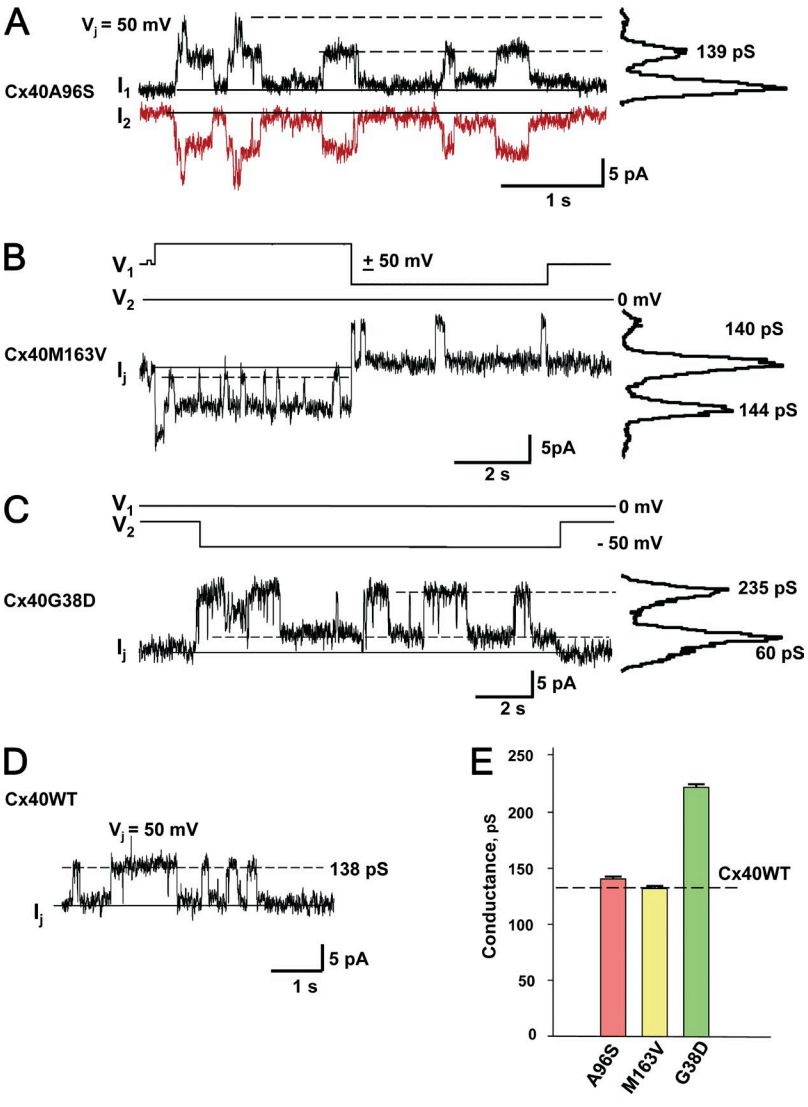

Figure 3. Single-channel properties of Cx40 mutant gap junctions. (A) Sister single-channel currents (I_1 and I_2) recorded from a N2A Cx40A96S cell pair during maintained V_j of 50 mV. Solid line, zero current level. The all-points current histogram (right-hand side) revealed a conductance of 139 pS. (B) Bipolar pulse protocol (V_1 and V_2) and associated single-channel current recording from a N2A Cx40M163V cell pair. The all-points current histogram yielded conductances of 140 and 144 pS for negative and positive V_j, respectively. (C) Voltage-pulse protocol (V_1 and V_2) and associated single-channel current (I_j) recorded from a N2ACx40G38 mutant cell pair. The all-points current histogram revealed 235-pS main state conductance and 60-pS residual conductance levels, respectively. (D) Single-channel current (I_j) recorded at the maintained V_j of 50 mV from a WT hCx40 N2A cell pair. The dashed line corresponds to an ∼138-pS conductance level. (E) Average of unitary conductances measured from A96S (139 ± 2 pS; n = 32), M136V (131 ± 2 pS; n = 32), and G38D (220 ± 3 pS; n = 67) cell pairs. The dashed line denotes the unitary conductance of WT Cx40 (135 ± 1.4 pS; n = 72). Error bars represent means ± SEM.

$P < 0.0001$, respectively), whereas the slope (i.e., permeability) of A96S was similar to that of the WT ($P = 0.2106$). In summary, the permeability of mutant gap junctions to LY exhibited the following order: G38D > M163V > A96S ≈ Cx40WT.

Fig. 5 shows the same protocol as in Fig. 4 using cationic EtBr to probe A96S permeability instead. Relative fluorescence intensity is plotted for the source and recipient cells of a pair (Fig. 5 B), as pictured in Fig. 5 A. For comparison's sake, an example of EtBr permeability for a cell pair expressing G38D is also included (Fig. 5 C). There is a significant fluorescence intensity increase delay in the recipient cell up to the ~6-min mark, suggesting the intercellular binding of a cationic probe. It is known that EtBr demonstrates pronounced binding to nucleic acids and when bound to DNA exhibits strong increase of fluorescence intensity (Lepecq and Paoletti, 1967; Alonso et al., 2006). Because of such restrictions, exact quantitative assessment of EtBr transfer is difficult, and therefore the data were used only for the qualitative comparison of mutant connexins. A96S has a significantly higher apparent permeability to EtBr than G38D, as depicted in Fig. 5 (B and C). A summary of the EtBr permeability data, as a function of junctional conductance, for all of the mutant and WT connexins for EtBr permeability is shown in Fig. 5 D.

The best fit of the data to the first-order regression produced the following slopes: $0.0384 \pm 0.0172\ nS^{-1}$ (M163V), $0.0304 \pm 0.0042\ nS^{-1}$ (A96S), $0.0013 \pm 0.0013\ nS^{-1}$ (G38D), and $0.0106 \pm 0.0016\ nS^{-1}$ (hCx40WT) for EtBr flux. Comparison of the slopes for M163V and A96S mutants revealed statistically higher permeability of these mutants to EtBr than WT hCx40 and rCx40 ($P < 0.001$). In contrast, G38D channels were almost impermeable to cationic EtBr, suggesting that G38D is responsible for altered channel selectivity. As a result, G38D mutant

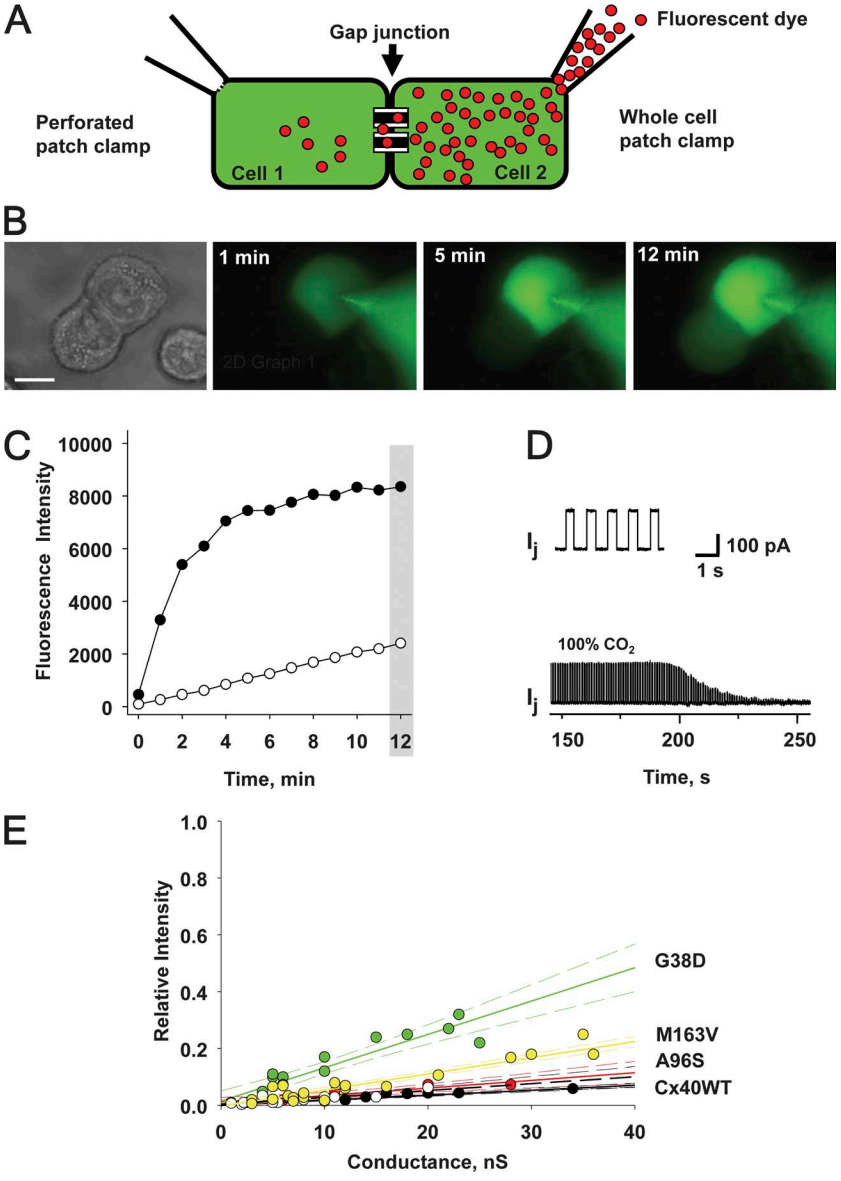

Figure 4. Methods to assess gap junction permeability. (A) Dual whole-cell and perforated-patch clamp has been used to assess gap junction conductance and to deliver the fluorescent probe to the donor cell (rightmost cell) of a pair. (B) LY flux between HeLaCx40G38D cells. Fluorescence emission is monitored over time (1-, 5-, and 12-min records shown) after an LY injection to the rightmost cell of a pair. Bar, 10 µm. (C) Plot of fluorescence intensity versus time for an injected cell (●) and a recipient cell (○). Shaded area indicates the 12-min time point at which the ratio of the recipient cell's fluorescence intensity to the source cell's fluorescence intensity was calculated. (D; top) I_j evoked by V_j pulses ($g_j = 18nS$). (Bottom) The application of 100% CO_2 produced a progressive decrease in I_j. (E) Summary plots of the relative fluorescence intensity versus g_j for LY in cells expressing Cx40 mutants: M163V (yellow circles), G38D (green circles), A96S (red circles), WT hCx40 (white circles), and WT rCx40 (black circles). Each data point corresponds to the relative fluorescence intensity (the ratio of the fluorescence intensity of the recipient cell over that of the injected cell) obtained at the 12-min time point after dye injection. Solid lines represent the first-order regressions, and dashed lines represent 95% confidence intervals.

channels exhibited significantly restricted transfer of EtBr compared with WT hCx40 and rCx40 (P = 0.0034–0.0041). In brief, M163V and A96S channels exhibited enhanced EtBr permeability, whereas G38D revealed diminished permeability, relative to WT Cx40: M163V > A96S > Cx40WT > G38D.

The simultaneous recording of fluorescence intensity of a probe and gap junction conductance allowed us to quantitatively estimate permeability of mutant connexins. Using the slope data in Figs. 4 E and 5 D, as well as methods described above and in Valiunas et al. (2002), Hernandez et al. (2007), and Kanaporis et al. (2008, 2011), we directly calculated the fluorescent probe flux rate (molecules/channel/s), the transfer rate of the fluorescent probe relative to the ubiquitous K^+ ions, and single-channel permeability ($P\gamma$) for all mutant connexins tested. The calculated probe fluxes of LY/EtBr for the mutant connexins yielded: 1,137 (LY)/16,156 (EtBr) molecules/channel/s for A96S; 7,757/1,121 for G38D; 2,242/19,218 for M163V, and 989/5,453 for hCx40WT. The LY and EtBr flux (molecules/channel/s) data for all the mutants in this study are summarized in Table 1.

Fig. 6 A shows summary data for single-channel permeability to LY and EtBr. The calculated mean $P\gamma$ ($cm^3/s \times 10^{-15}$) for LY yielded the following values for the mutant connexins: 0.95 ± 0.17 (A96S; $n = 6$), 6.52 ± 0.72 (G38D; $n = 15$), and 1.87 ± 0.11 (M163V; $n = 24$). The data show that $P\gamma$ to LY for A96S mutant was similar to the WT hCx40 (0.82 ± 0.17; $n = 12$), whereas M163V and G38D mutant channels exhibited approximately two and approximately eight times higher unitary permeability than the WT hCx40, respectively. In HeLa cells expressing mutants A96S and M163V, calculated $P\gamma$ ($cm^3/s \times 10^{-15}$) for EtBr yielded similar values: 10.91 ± 1.52 (A96S; $n = 7$) and 13.08 ± 5.85 (M163V; $n = 9$), which were significantly higher (P < 0.0001) than those of the WT hCx40 (3.61 ± 0.56; $n = 5$). However, the $P\gamma$

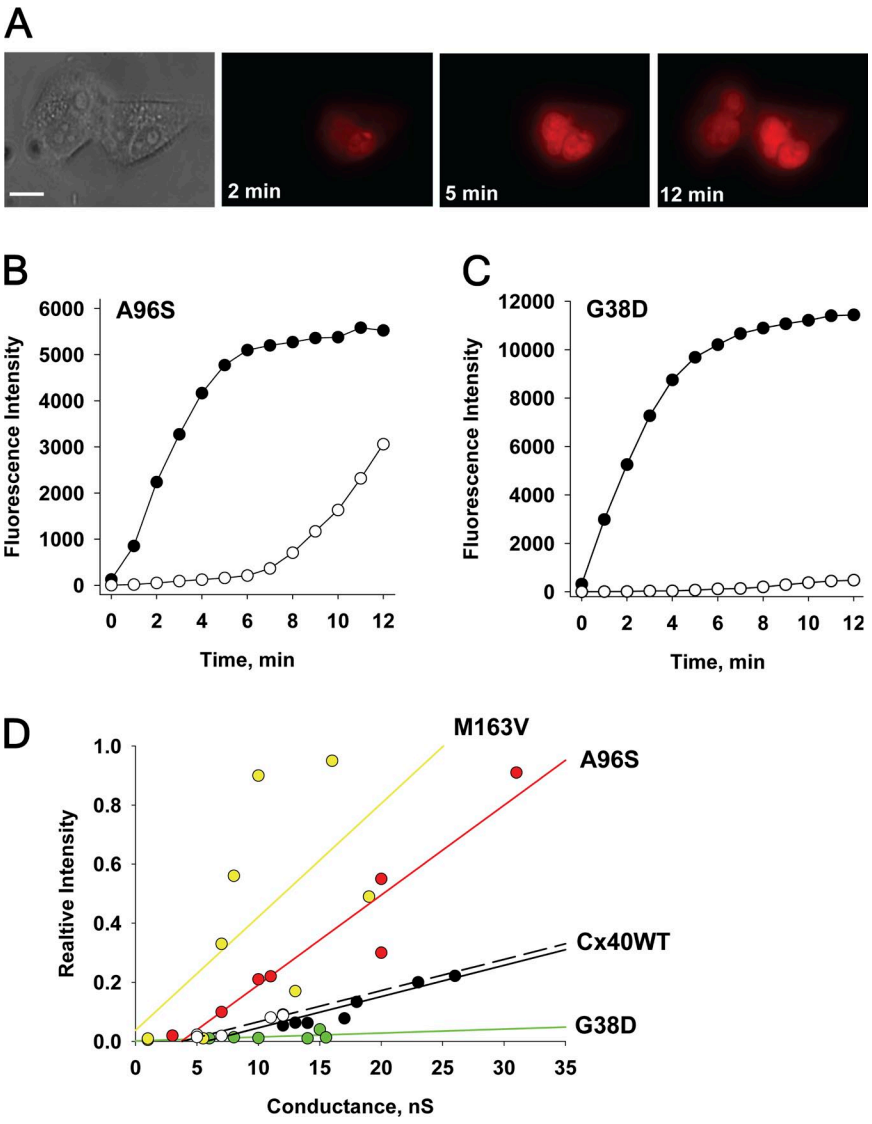

Figure 5. Cell-to-cell transfer of EtBr. (A) EtBr flux between a HeLaCx40A96S cell pair. Epifluorescent images taken at 2-, 5-, and 12-min marks after dye injection into the rightmost cell. Bar, 10 µm. Plots of fluorescence intensity versus time for an injected cell (●) and a recipient cell (○) obtained from A96S (B) and G38D (C) mutant pairs. g_j of 20 and 15 nS was measured at the end of dye transfer. Note a significant fluorescence intensity increase delay in the recipient cell (B) caused by intracellular binding. (D) Summary plots of the relative fluorescence intensity versus g_j for EtBr in cells expressing Cx40 mutants: G38D (green circles), A96S (red circles), M163 V (yellow circles), WT hCx40 (white circles), and WT rCx40 (black circles). Solid lines are the first-order regressions.

of G38D mutants (0.73 ± 0.71; $n = 6$) was significantly smaller compared with the WT.

Fig. 6 B compares LY and EtBr permeability of WT and mutant connexins, relative to K^+ ions. The colored bars represent LY/K^+ and EtBr/K^+ ratios plotted on a log scale for A96S (pink bar), M163V (yellow bar), G38D (green bar), hCx40WT (gray bar), and rCx40WT (black bar). Both M163V and G38D mutant gap junctions had elevated permeability to anionic LY relative to K^+ ions when compared with the WT Cx40, whereas

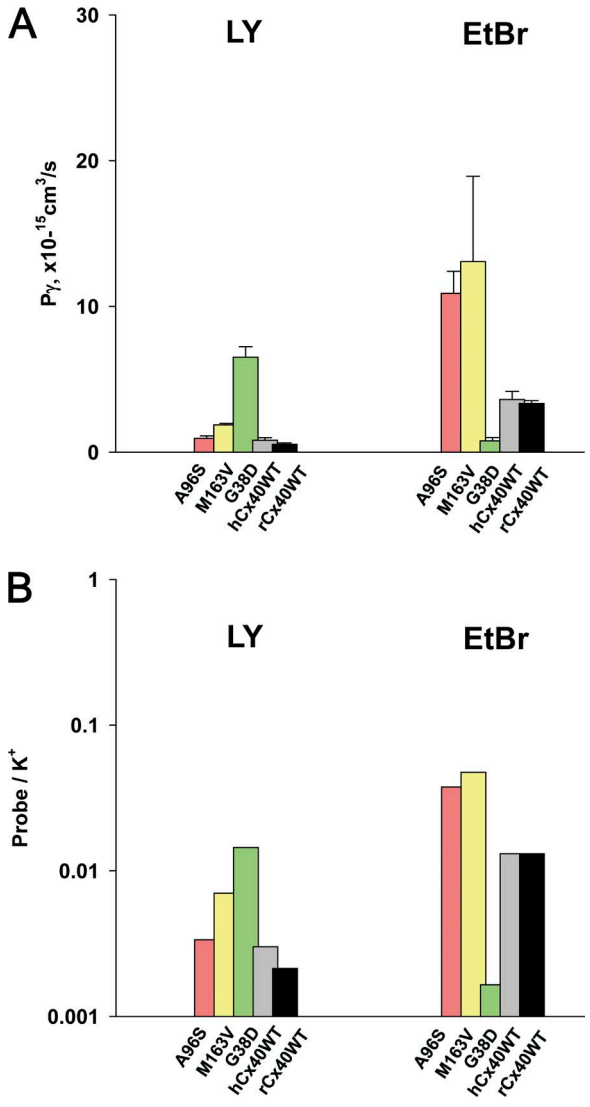

Figure 6. Permeability properties of mutant connexins. (A) Summary of single-channel permeability (Pγ) for mutants and WT Cx40 gap junction channels to LY and EtBr: A96S (pink bar), M163V (yellow bar), G38D (green bar), hCx40WT (gray bar), and rCx40WT (black bar). Refer to Results and Table 1 for further information. (B) Permeability of fluorescent probes relative to K^+ ions for mutants and WT Cx40: A96S (pink bar), M163V (yellow bar), G38D (green bar), hCx40WT (gray bar), and rCx40WT (black bar). The bars represent probe/K^+ ratios plotted on a log scale. See Table 1 and Results for details. Error bars represent means ± SEM.

A96S LY transfer was similar to that of the WT: M163V > G38D > A96S ≈ Cx40WT.

Table 1 contains all of the calculated permeability parameters for LY and EtBr, along with unitary conductance, macroscopic conductance, and parameters determined by the Boltzmann fit: $V_{j,o}$, $g_{j,min}$, and z. The calculated values for EtBr follow a trend consistent with previously published data for WT rCx40 (Kanaporis et al., 2011). It should be noted that changes in fluorescence efficiency, upon binding to DNA, make quantification of EtBr less reliable than that of LY. Regardless, comparison of the EtBr apparent permeability among the three mutants uses only the mutants as the significant variables. The low apparent EtBr cation permeability of G38D suggests the possibility of EtBr having significant interactions with charged moieties within the channel, presumably at site 38.

DISCUSSION

Gap junctions composed of Cx40, and to a lesser degree Cx43 and Cx45, within the atrium are responsible for the longitudinal spread of current that is generated by the propagating action potential originating in the SA node. Alteration of longitudinal current flow is one very plausible way to cause reentrant arrhythmias (Spach and Josephson, 1994; Hall and Gourdie, 1995; Wit and Peters, 2012). Reduction of longitudinal current flow can arise from: (a) a reduction in the number of functional gap junction channels within the intercalated disc; (b) a lateral redistribution of those channels; or (c) the introduction of a mutant that might cause either (a) and/or (b), but may also affect channel open probability, voltage dependence, or permeability. In addition, when heterologously expressed, a mutated form can act as a dominant negative by slowing or reducing the trafficking efficiency of WT connexins.

The data presented in this study demonstrate that all investigated Cx40 mutations can form functional gap junction channels. We found that in our experimental conditions, all three mutants exhibited a range of macroscopic coupling ranging from 0.5 to 40 nS and were all comparable with the WT hCx40 conductance (Table 1). Gollob et al. (2006) coexpressed human Cx40A96S with WT Cx40 in oocytes and found that A96S was able to effectively reduce junctional conductance to approximately one third of the conductance for Cx40 alone. In that study, junctional conductance for homotypic Cx40A96S averaged 1.8 versus 16.5 nS for the WT, when expressed in N2A cells. In contrast, Patel et al. (2014) reported lower level (4.8-nS) coupling for the WT Cx40 in the same expression system (N2A cells), and subsequently higher conductances for mutants G38D (9.69 nS) and M163V (6.81 nS). A recent study by Lübkemeier et al. (2013), using mouse A96S, also found that junctional conductance was reduced

significantly relative to the control and attributed this to low open probability. They also found that voltage dependence was different than for the WT. When human Cx40A96S was homotypically expressed in N2A cells, we found only a slightly lowered junctional conductance relative to the human Cx40 control, although it was not the case when expressed in HeLa cells. The reduction in junctional conductance was much less severe than that reported by Lübkemeier et al. (2013; ∼18% reduction for human [Table 1] vs. ∼30× reduction for mouse). Moreover, human A96S voltage dependence was the same as for WT (Fig. 2).

To compare coupling and voltage-gating properties of both mutants, hA96S and mA96S, we performed experiments with the same HeLa mCx40A96S cell line (obtained from K. Willecke, University of Bonn, Bonn, Germany) and our own standard experimental protocols and conditions.

Fig. 7 summarizes our results obtained from the HeLa mCx40A96S cell pairs, which essentially reproduced the data reported by Lübkemeier et al. (2013) (i.e., low sensitivity to voltage and low coupling). Fig. 7 A shows an example of gap junction currents (I_j) elicited by a bipolar pulse protocol from a HeLa mCx40A96S cell pair. The associated gap junction currents (I_j) increased proportionally with V_j, exhibiting very weak voltage- and time-dependent deactivation for positive and negative V_j. Fig. 7 B summarizes the normalized steady-state conductance data gathered from six HeLa cell pairs expressing mCx40A96S. The data were fitted to a Boltzmann equation with the following parameters: $V_{j,o}$ = 85 mV, $g_{j,min}$ = 0.71, and z = 1.1. The g_j–V_j relationship was similar to that reported in Lübkemeier et al. (2013), with high $V_{j,o}$ and $g_{j,min}$ values. However, direct quantitative comparison of parameters is difficult because of the use of different fitting models in data analysis. Mouse A96S mutants exhibited a lower range of macroscopic junctional conductance (g_j) from 0.1 to 8 nS, and the averaged total conductance (1.7 ± 0.2 nS; n = 64) was significantly lower (P < 0.001) than that measured from human A96S junctions (8.9 ± 1.5 nS; n = 34; Fig. 7 C). The junctional conductance for mouse A96S channels reported by Lübkemeier et al. (2013) was similarly low (∼1.3 nS). Fig. 7 D shows an example of a single-channel recording from a HeLa mCxA96S cell pair. The all-point current histograms revealed a conductance of 149 pS for mCx40A96S, similar to the unitary conductance (∼165 pS) reported by Lübkemeier et al. (2013), when taking into account the different pipette solutions used in both studies.

The amino acid sequence for mouse Cx40 is 83% identical when compared with human Cx40. The amino acid sequence for WT mouse Cx40 and WT human Cx40 is identical from positions 10 to 115 without any interruption. The next longest undisturbed sequence identity occurs between positions 181 and 211. Many of the non-identical regions occur in the C terminus. The difference in functional behavior for the WTs suggests

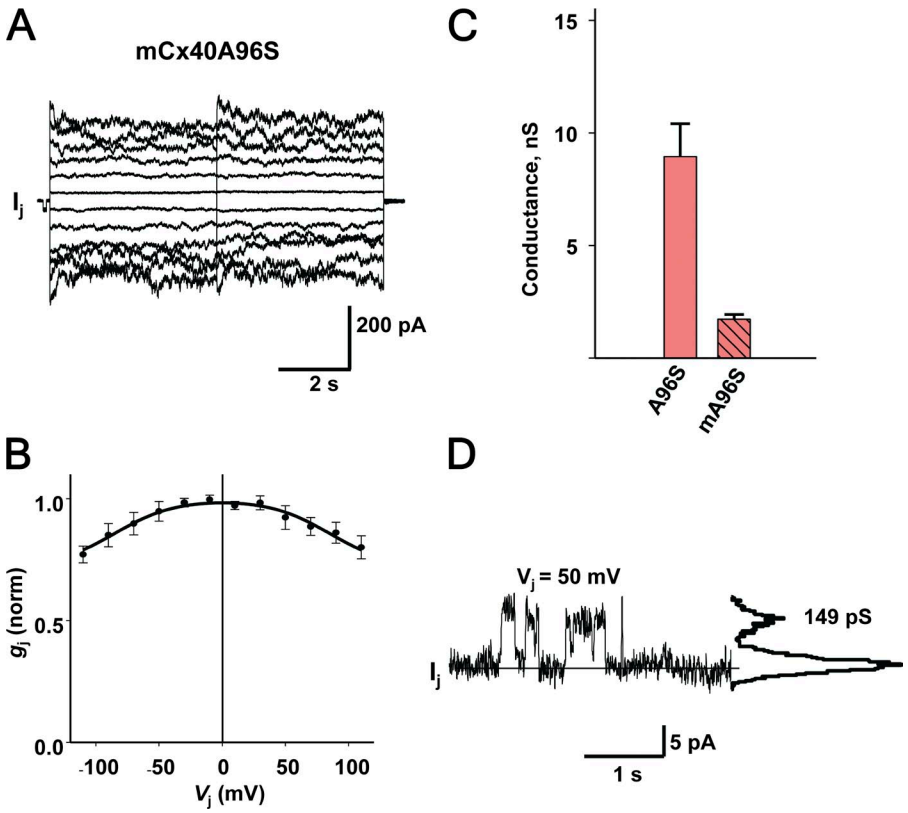

Figure 7. Functional properties of mouse Cx40 A96S gap junctions. (A) Gap junction currents (I_j) recorded from a HeLa cell pair transfected with mCx40A96S in response to a 5-s bipolar pulse from ±10 to ±110 mV using increments of 20 mV. (B) Summary plot of normalized g_j versus V_j. The continuous black line represents the best fit of the data to the Boltzmann equation ($V_{j,o}$ = 85 mV, $g_{j,min}$ = 0.71, and z = 1.1; n = 6). (C) Averaged total conductance measured from human A96S (8.9 ± 1.5 nS; n = 34; pink bar) and mouse A96S (1.7 ± 0.2 nS; n = 64; pink striped bar) junctions (P < 0.001; Mann–Whitney rank-sum test). (D) Single-channel currents (I_j) recorded from a HeLa mCx40A96S cell pair maintained at V_j of 50 mV. Solid line, zero current level. The all-points current histogram (right-hand side) revealed a conductance of 149 pS. Error bars represent means ± SEM.

that the single-site mutation (A96S) altered tertiary structure differently in the mouse than in the human mutant, affecting both trafficking and voltage dependence more severely in the mouse mutant. The discrepancies among different studies in reported macroscopic junctional conductance for mutants and WT Cx40 may likely be attributed to differences in various factors such as expression systems and procedures, transfection vectors and plasmids, sample pool size, experimental conditions, and pipette and bath solutions. Finally, the different gating behavior of mouse and human A96S connexins implies that direct comparison for the purposes of studying pathologies such as atrial fibrillation is less than optimal.

The unitary conductance for each of the two mutants, M163V and A96S, was similar to WT Cx40 (Table 1). However, G38D had a unitary conductance ∼1.6–1.7 times that of WT or the other mutants (220 vs. 131–139 pS). The much larger unitary conductance of G38D suggests that the M1/E1 regions are indeed significant parts of the pore wall. The G38D is located at the extracellular end of M1 (Fig. 1 A) and replaces the smallest and most flexible amino acid (Gly) with one (Asp) that is large, stiff, and negatively charged. This substitution may cause additional electrostatic interactions as well as loss of flexibility. The Gly may be a functionally relevant hinge, considering that M1 is the most rigid domain of the connexin (Zonta et al., 2012) and E1 must interface with the other cell, which may require flexibility. Bearing that in mind, the G38D mutation in the M1 domain may affect the shape, charge, and hydrophobicity of the pore, thus altering the unitary conductance of the channel. For example, the analogous G551D and G1349D mutations in a CFTR chloride channel caused a misregulation of the channel (Welsh and Smith, 1993). Recently, Patel et al. (2014) also reported 20% larger unitary conductance for G38D channels. Additionally, they reported that G38D mutant channels were more voltage sensitive (V_j = 34 mV) than the ones reported in this study. However, direct comparison is difficult, as different experimental conditions were used in both studies: N2A cells versus HeLa cells, ramp protocol versus voltage step protocol, and KCl versus KAsp pipette solution. Also, it has been shown that the ionic composition of the pipette solution affects the kinetics of gap junction currents (Valiunas et al., 2000).

The increased conductance is inconsistent with a reentrant arrhythmia where reduced longitudinal current is considered to be the cause. If homotypic G38D channels were expressed more robustly along the lateral surfaces, longitudinal current would be reduced and potentially allow the onset of a reentrant arrhythmia (Peters et al., 1997; Cabo et al., 2006).

All three mutants had altered permeability characteristics relative to the WT Cx40. G38D gap junctions demonstrated an approximately fivefold enhanced anionic probe permeability (LY/K^+ = 0.0145 vs. 0.0030) but suppressed cationic probe permeability to a near impermeable level ($EtBr/K^+$ = 0.0016 vs. 0.0131). The apparent contradiction of a higher unitary conductance for G38D, presumed to be the result of increased cation (K^+) and anion ($aspartate^-$) fluxes, whereas cationic probe (EtBr) flux is reduced, argues that the mobility of EtBr is compromised as a result of charge to charge interactions while accessing the channel pore or within the pore. Alternatively, the mutation could be either a binding site to EtBr, or it has caused a significant enough structural alteration to allow partial occlusion, which results in binding or entrapment elsewhere in the pore, without significantly affecting the mobility of the smaller K^+. The substitution of a short, neutral, and flexible Gly in exchange for a large, rigid, and negative Asp may alter the interactions of the solute with the pore walls as a result of modified pore size and/or varied charge interface. The reduced unitary conductance cannot account for the strong reduction in cation permeability alone, but most certainly it is a contributing factor.

The increased anionic LY permeability and reduced cationic EtBr permeability brought on by the substitution of an aliphatic amino acid for a negatively charged amino acid in G38D significantly alters Cx40 selectivity. How this altered selectivity might be a factor in arrhythmogenic activity is not clear. Although, for G38D, enhanced permeability to cAMP, as implied by the elevated anionic LY permeability, could be sufficient to result in augmented spread of cAMP from a source cell triggering pacing activity within adjacent cells via activation of L-type calcium channels or normally dormant HCN channels. A recent study by Molina et al. (2012) suggests that control of intracellular cAMP by cyclic adenosine monophosphate phosphodiesterase type 4 is an essential component in limiting vulnerability to arrhythmias. The enhanced anionic LY permeability of M163V suggests that it might also affect arrhythmogenic activity in a similar fashion. Enhanced cell to cell diffusion of anionic second messengers such as IP_3 might also be expected to promote arrhythmogenic activity through increased activity of L-type calcium channels. In contrast, suppressed cationic probe permeability, as noted with G38D, would be predicted to reduce calcium permeability and thus reduce arrhythmogenic activity (Podzuweit et al., 1980; Dzhura et al., 2000; Kamp and Hell, 2000).

The M163V channels exhibited ∼2.3 times higher anionic LY permeability than the WT hCx40 (LY/K^+ = 0.007 vs. 0.0030). M163V also had enhanced cationic EtBr permeability ($EtBr/K^+$ = 0.047 vs. 0.0131). The increase in permeability to both cationic and anionic solutes suggests that this mutation nonspecifically reduces selectivity of the channel, as neither unitary channel conductance nor macroscopic conductance was affected. In M163V, the large, hydrophobic, and nonreactive Met

is changed to a hydrophobic but small Val. It is not clear how such a mutation would affect permeability as M163V faces membrane lipids. The A96S mutation is located on the pore-facing side of M2 domain close to intercellular loop, CL (Fig. 1 A). Although LY transfer ($LY/K^+ = 0.0034$) was similar to that of the WT, A96S channels were more permeable to cations than the WT channels were ($EtBr/K^+ = 0.0376$ vs. 0.0131). Enhanced cationic EtBr permeability would suggest that these two mutants (M163V and A96S) might allow increased calcium transfer from cell to cell resulting in up-regulated L-type channel activity (Kamp and Hell, 2000), which has the potential to create arrhythmogenic activity.

Characterization of channel permselectivity offers insights into the function of intercellular communication in mutated gap junctions. We have already reported that Cx26 mutations (T8M and N206S) associated with deafness showed altered permeability to cationic molecules (Meşe et al., 2008). The ability of different connexins to permit or discriminate against the passage of the second messengers such as cAMP, cGMP, or IP_3 has been well documented (Bevans et al., 1998; Bedner et al., 2006; Hernandez et al., 2007; Kanaporis et al., 2008). Interestingly, compared with mutant channel properties reported in this study, it has also been reported that Cx26 mutation V84L, associated again with deafness, reduces IP_3 permeability without changes in unitary channel conductance or macroscopic coupling (Beltramello et al., 2005).

The permeability data for the three mutants suggests a potential role for all three mutants with regard to arrhythmogenesis where enhanced distribution of secondary messengers would be a potentially deleterious factor promoting arrhythmia. It is also possible that the differences in permeability illustrated here are not the major determining feature affecting arrhythmias as noted in previous studies, where the mutant forms G38D and M163V displayed a different, mosaic-like pattern of distribution with biopsied human atrial tissue samples (Gollob et al., 2006). The immunostaining data of Gollob et al. (2006) suggest another, as of yet, untested possibility of altered trafficking of the mutants relative to WT Cx40. For example, altered trafficking of the mutants could result in extensive lateralization or reduction of the junctional conductance at the intercalated disc, reducing longitudinal current flow and as a consequence creating the potential for reentrant arrhythmias (Spach and Josephson, 1994; Hall and Gourdie, 1995; Wit and Peters, 2012). Another variant on lateralization is not an alteration in junctional conductance but an alteration in the permeability of second messengers to adjacent cells perpendicular to the long axis of the tissue. As already noted, the diffusion of second messengers to laterally placed adjacent cells might activate L-type calcium channels or other processes causing excitation inhomogeneity, which could result in reentrant arrhythmias. If an increase in lateralization manifested either as an increased junctional conductance or permeability, or both, then reduced anisotropy of the myocardium effectively would result in dilution of the directional dependence of the tissue and the magnitude of the longitudinal current.

The authors thank Dr. K. Willecke for providing HeLa mCx40A96S cells.

This work was supported by the National Institutes of Health (grants GM088181 to V. Valiunas, GM88180 to P.R. Brink, and AR59505 to T.W. White).

The authors declare no competing financial interests.

Kenton J. Swartz served as editor.

Submitted: 14 July 2015
Accepted: 23 September 2015

REFERENCES

Alonso, A., M.J. Almendral, Y. Curto, J.J. Criado, E. Rodríguez, and J.L. Manzano. 2006. Determination of the DNA-binding characteristics of ethidium bromide, proflavine, and cisplatin by flow injection analysis: usefulness in studies on antitumor drugs. *Anal. Biochem.* 355:157–164. http://dx.doi.org/10.1016/j.ab.2006.06.004

Beblo, D.A., H.Z. Wang, E.C. Beyer, E.M. Westphale, and R.D. Veenstra. 1995. Unique conductance, gating, and selective permeability properties of gap junction channels formed by connexin40. *Circ. Res.* 77:813–822. http://dx.doi.org/10.1161/01.RES.77.4.813

Bedner, P., H. Niessen, B. Odermatt, M. Kretz, K. Willecke, and H. Harz. 2006. Selective permeability of different connexin channels to the second messenger cyclic AMP. *J. Biol. Chem.* 281:6673–6681. http://dx.doi.org/10.1074/jbc.M511235200

Beltramello, M., V. Piazza, F.F. Bukauskas, T. Pozzan, and F. Mammano. 2005. Impaired permeability to Ins(1,4,5)P3 in a mutant connexin underlies recessive hereditary deafness. *Nat. Cell Biol.* 7:63–69. http://dx.doi.org/10.1038/ncb1205

Bevans, C.G., M. Kordel, S.K. Rhee, and A.L. Harris. 1998. Isoform composition of connexin channels determines selectivity among second messengers and uncharged molecules. *J. Biol. Chem.* 273: 2808–2816. http://dx.doi.org/10.1074/jbc.273.5.2808

Bukauskas, F.F., C. Kempf, and R. Weingart. 1992. Cytoplasmic bridges and gap junctions in an insect cell line (Aedes albopictus). *Exp. Physiol.* 77:903–911. http://dx.doi.org/10.1113/expphysiol.1992.sp003657

Bukauskas, F.F., C. Elfgang, K. Willecke, and R. Weingart. 1995. Biophysical properties of gap junction channels formed by mouse connexin40 in induced pairs of transfected human HeLa cells. *Biophys. J.* 68:2289–2298. http://dx.doi.org/10.1016/S0006-3495(95)80411-X

Cabo, C., J. Yao, P.A. Boyden, S. Chen, W. Hussain, H.S. Duffy, E.J. Ciaccio, N.S. Peters, and A.L. Wit. 2006. Heterogeneous gap junction remodeling in reentrant circuits in the epicardial border zone of the healing canine infarct. *Cardiovasc. Res.* 72:241–249. http://dx.doi.org/10.1016/j.cardiores.2006.07.005

Christophersen, I.E., H.N. Holmegard, J. Jabbari, A. Sajadieh, S. Haunsø, A. Tveit, J.H. Svendsen, and M.S. Olesen. 2013. Rare variants in GJA5 are associated with early-onset lone atrial fibrillation. *Can. J. Cardiol.* 29:111–116. http://dx.doi.org/10.1016/j.cjca.2012.08.002

Davis, L.M., M.E. Rodefeld, K. Green, E.C. Beyer, and J.E. Saffitz. 1995. Gap junction protein phenotypes of the human heart and conduction system. *J. Cardiovasc. Electrophysiol.* 6:813–822. http://dx.doi.org/10.1111/j.1540-8167.1995.tb00357.x

Dzhura, I., Y. Wu, R.J. Colbran, J.R. Balser, and M.E. Anderson. 2000. Calmodulin kinase determines calcium-dependent facilitation of L-type calcium channels. *Nat. Cell Biol.* 2:173–177. http://dx.doi.org/10.1038/35004052

Fan, J.S., and P. Palade. 1998. Perforated patch recording with beta-escin. *Pflugers Arch.* 436:1021–1023. http://dx.doi.org/10.1007/PL00008086

Gollob, M.H., D.L. Jones, A.D. Krahn, L. Danis, X.Q. Gong, Q. Shao, X. Liu, J.P. Veinot, A.S. Tang, A.F. Stewart, et al. 2006. Somatic mutations in the connexin 40 gene (GJA5) in atrial fibrillation. *N. Engl. J. Med.* 354:2677–2688. http://dx.doi.org/10.1056/NEJMoa052800

Gros, D., T. Jarry-Guichard, I. Ten Velde, A. de Maziere, M.J. van Kempen, J. Davoust, J.P. Briand, A.F. Moorman, and H.J. Jongsma. 1994. Restricted distribution of connexin40, a gap junctional protein, in mammalian heart. *Circ. Res.* 74:839–851. http://dx.doi.org/10.1161/01.RES.74.5.839

Hall, J.E., and R.G. Gourdie. 1995. Spatial organization of cardiac gap junctions can affect access resistance. *Microsc. Res. Tech.* 31:446–451. http://dx.doi.org/10.1002/jemt.1070310513

Hernandez, V.H., M. Bortolozzi, V. Pertegato, M. Beltramello, M. Giarin, M. Zaccolo, S. Pantano, and F. Mammano. 2007. Unitary permeability of gap junction channels to second messengers measured by FRET microscopy. *Nat. Methods.* 4:353–358.

Jansen, J.A., T.A. van Veen, J.M. de Bakker, and H.V. van Rijen. 2010. Cardiac connexins and impulse propagation. *J. Mol. Cell. Cardiol.* 48:76–82. http://dx.doi.org/10.1016/j.yjmcc.2009.08.018

Kamp, T.J., and J.W. Hell. 2000. Regulation of cardiac L-type calcium channels by protein kinase A and protein kinase C. *Circ. Res.* 87:1095–1102. http://dx.doi.org/10.1161/01.RES.87.12.1095

Kanaporis, G., G. Mese, L. Valiuniene, T.W. White, P.R. Brink, and V. Valiunas. 2008. Gap junction channels exhibit connexin-specific permeability to cyclic nucleotides. *J. Gen. Physiol.* 131:293–305. http://dx.doi.org/10.1085/jgp.200709934

Kanaporis, G., P.R. Brink, and V. Valiunas. 2011. Gap junction permeability: selectivity for anionic and cationic probes. *Am. J. Physiol. Cell Physiol.* 300:C600–C609. http://dx.doi.org/10.1152/ajpcell.00316.2010

Kanter, H.L., J.G. Laing, E.C. Beyer, K.G. Green, and J.E. Saffitz. 1993. Multiple connexins colocalize in canine ventricular myocyte gap junctions. *Circ. Res.* 73:344–350. http://dx.doi.org/10.1161/01.RES.73.2.344

Kostin, S., G. Klein, Z. Szalay, S. Hein, E.P. Bauer, and J. Schaper. 2002. Structural correlate of atrial fibrillation in human patients. *Cardiovasc. Res.* 54:361–379. http://dx.doi.org/10.1016/S0008-6363(02)00273-0

Lepecq, J.-B., and C. Paoletti. 1967. A fluorescent complex between ethidium bromide and nucleic acids: Physical-chemical characterization. *J. Mol. Biol.* 27:87–106. http://dx.doi.org/10.1016/0022-2836(67)90353-1

Lübkemeier, I., R. Andrié, L. Lickfett, F. Bosen, F. Stöckigt, R. Dobrowolski, A.M. Draffehn, J. Fregeac, J.L. Schultze, F.F. Bukauskas, et al. 2013. The Connexin40A96S mutation from a patient with atrial fibrillation causes decreased atrial conduction velocities and sustained episodes of induced atrial fibrillation in mice. *J. Mol. Cell. Cardiol.* 65:19–32. http://dx.doi.org/10.1016/j.yjmcc.2013.09.008

Meşe, G., V. Valiunas, P.R. Brink, and T.W. White. 2008. Connexin26 deafness associated mutations show altered permeability to large cationic molecules. *Am. J. Physiol. Cell Physiol.* 295:C966–C974. http://dx.doi.org/10.1152/ajpcell.00008.2008

Molina, C.E., J. Leroy, W. Richter, M. Xie, C. Scheitrum, I.O. Lee, C. Maack, C. Rucker-Martin, P. Donzeau-Gouge, I. Verde, et al. 2012. Cyclic adenosine monophosphate phosphodiesterase type 4 protects against atrial arrhythmias. *J. Am. Coll. Cardiol.* 59:2182–2190. http://dx.doi.org/10.1016/j.jacc.2012.01.060

Patel, D., J. Gemel, Q. Xu, A.R. Simon, X. Lin, A. Matiukas, E.C. Beyer, and R.D. Veenstra. 2014. Atrial fibrillation-associated connexin40 mutants make hemichannels and synergistically form gap junction channels with novel properties. *FEBS Lett.* 588:1458–1464. http://dx.doi.org/10.1016/j.febslet.2014.01.010

Peters, N.S., J. Coromilas, N.J. Severs, and A.L. Wit. 1997. Disturbed connexin43 gap junction distribution correlates with the location of reentrant circuits in the epicardial border zone of healing canine infarcts that cause ventricular tachycardia. *Circulation.* 95:988–996. http://dx.doi.org/10.1161/01.CIR.95.4.988

Podzuweit, T., G.C. Louw, and B.C. Shanley. 1980. Catecholamine/cyclic AMP/Ca^{2+} induces arrhythmias in the healthy pig heart. *Adv. Myocardiol.* 2:133–143.

Roberts, R. 2006. Genomics and cardiac arrhythmias. *J. Am. Coll. Cardiol.* 47:9–21. http://dx.doi.org/10.1016/j.jacc.2005.08.059

Saffitz, J.E. 2006. Connexins, conduction, and atrial fibrillation. *N. Engl. J. Med.* 354:2712–2714. http://dx.doi.org/10.1056/NEJMe068088

Spach, M.S., and M.E. Josephson. 1994. Initiating reentry: The role of nonuniform anisotropy in small circuits. *J. Cardiovasc. Electrophysiol.* 5:182–209. http://dx.doi.org/10.1111/j.1540-8167.1994.tb01157.x

Valiunas, V., R. Vogel, and R. Weingart. 2000. The kinetics of gap junction currents are sensitive to the ionic composition of the pipette solution. *Pflugers Arch.* 440:835–842. http://dx.doi.org/10.1007/s004240000376

Valiunas, V., J. Gemel, P.R. Brink, and E.C. Beyer. 2001. Gap junction channels formed by coexpressed connexin40 and connexin43. *Am. J. Physiol. Heart Circ. Physiol.* 281:H1675–H1689.

Valiunas, V., E.C. Beyer, and P.R. Brink. 2002. Cardiac gap junction channels show quantitative differences in selectivity. *Circ. Res.* 91:104–111. http://dx.doi.org/10.1161/01.RES.0000025638.24255.AA

Vozzi, C., E. Dupont, S.R. Coppen, H.I. Yeh, and N.J. Severs. 1999. Chamber-related differences in connexin expression in the human heart. *J. Mol. Cell. Cardiol.* 31:991–1003. http://dx.doi.org/10.1006/jmcc.1999.0937

Welsh, M.J., and A.E. Smith. 1993. Molecular mechanisms of CFTR chloride channel dysfunction in cystic fibrosis. *Cell.* 73:1251–1254. http://dx.doi.org/10.1016/0092-8674(93)90353-R

Wit, A.L., and N.S. Peters. 2012. The role of gap junctions in the arrhythmias of ischemia and infarction. *Heart Rhythm.* 9:308–311. http://dx.doi.org/10.1016/j.hrthm.2011.09.056

Zonta, F., G. Polles, G. Zanotti, and F. Mammano. 2012. Permeation pathway of homomeric connexin 26 and connexin 30 channels investigated by molecular dynamics. *J. Biomol. Struct. Dyn.* 29:985–998. http://dx.doi.org/10.1080/073911012010525027